Removal of mercury ions from aqueous solutions by crosslinked chitosan-based adsorbents: a mini review

Dan Zhang, Grégorio Crini, Eric Lichtfouse, Baker Rhimi, Chuanyi Wang

The Chemical Record 20, 1-16, 2020
https://doi.org/10.1002/tcr.202000073

Removal of Mercury Ions from Aqueous Solutions by Crosslinked Chitosan-based Adsorbents: A Mini Review

Dan Zhang,[a] Grégorio Crini,[b] Eric Lichtfouse,[c, d] Baker Rhimi,[a] and Chuanyi Wang*[a]

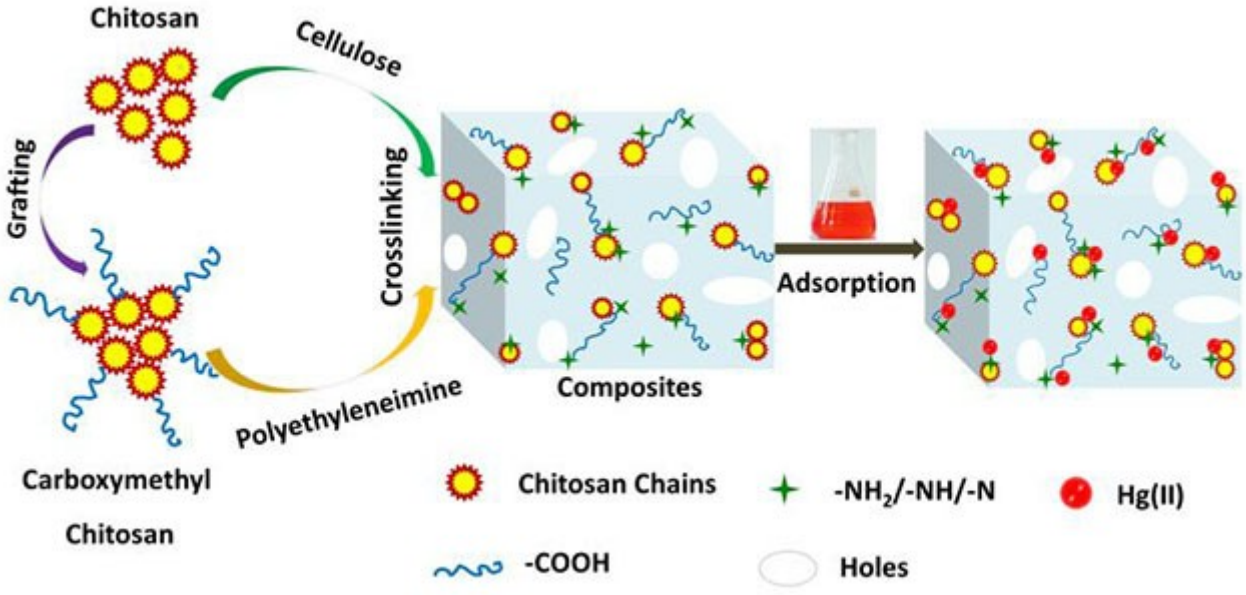

Abstract: Abatement of mercury emissions in air and waters has become a global challenge due to the toxicity of mercury species for life, yet actual remediation techniques are limited. In particular, adsorption of mercury ions onto solids is widely used but most adsorption techniques are not specific, and in turn, removal efficiency is lower. Adsorbents developed so far include activated carbon, clay, bentonite, cellulose and chitosan. Chitosan derivatives have recently attracted research attention for water purification because their molecular frames contain a large amount of $-NH_2$ and –OH groups that can chelate with metal ions specifically. This manuscript reviews recent advances in chitosan-based adsorbents designed to remove mercury ions from wastewater. Focus is placed on their design, synthesis, characterization, adsorption properties, adsorption mechanisms and applications.

Keywords: Mercury ions removal, Chitosan-based adsorbents, Adsorption mechanism, Environmental remediation

1. Introduction

Mercury is a metallic element displaying persistent, bioaccumulative and bio-expanding toxic effects.[1] It is known as a mutagen, teratogen and carcinogen that may cause embryo death, cytochemistry and histopathological effects.[2] Indeed, pollution by mercury has already led to major alteration of human health and the environment.[3] The toxicity of mercury depends to a large extent on its chemical state.[4] For instance, Hg(II) is the most toxic form of mercury because Hg(II) can bind to the cysteine amino acid of proteins and, in turn, may induce protein inactivation and degeneration.[5] Moreover, the toxicity of mercury is enhanced by bioaccumulation in organisms and by bio-transmission through the food chain, a classical phenomenon being the concentration of mercury in fish species located at high trophic levels, e. g., swordfish, king mackerel and albacore tuna.[6] The major sources of mercury emissions include natural sources and human activities, such as volcanic eruptions, combustion of fossil fuels, coal, mining and mineral processing.[7,8] As a consequence, there is a need for efficient methods to abate mercury pollution.

Common methods for removing mercury ions from wastewater include chemical precipitation, coagulation, ion exchange, membrane filtration and adsorption.[9–13] Nonetheless, those methods are often limited by high cost, long response time, tedious operation and post-processing, and inability to meet emission standards.[14] Adsorption is widely used for removing mercury ions from industrial wastewaters, yet there are actually few adsorbents that are selective to mercury,[15–17] which is a major issue because mercury ions usually coexist with other abundant ions in wastewater.[18,19] The main adsorbents for mercury ions removal include activated carbon, clay, polymeric materials, cellulose, starch and chitosan.[20–25] As a versatile, low cost and green product,[26,27] chitosan has drawn great attention, and it has been extensively studied and applied in the chemical industry, agriculture, cosmetics, pharmacy, and biomedical engineering.[28–31] In addition, chitosan derivatives have also been used for the treatment of wastewater, especially for coagulation-flocculation, metal extraction and recovery and dye removal.[32,33]

Chitosan is an amino-polysaccharide containing a large number of amino ($-NH_2$) and hydroxyl (–OH) groups, which confer chitosan a high adsorption capacity and selectivity to mercury ions.[34] Chitosan displays high metal-binding affinity in either concentrated or diluted effluents. Moreover, chitosan is non-toxic, biocompatible and can be used in various forms such as beads, membranes, fibers and sponges.[35,36] Also, as a semi-flexible, hydrophilic and reactive biopolymer, chitosan can be easily modified chemically.[37]

Elucidation of adsorption mechanisms is critically important to understanding adsorption processes.[38] In general, adsorption mechanisms could be tackled by studying rate-controlling steps, kinetics, thermodynamics and isotherms in conjunction with spectroscopic analysis.[39–42] For chitosan, paired electrons of O and N from carboxyl and amino groups provide empty atomic orbitals and conditions for complexation between chitosan and heavy metal ions.[43] Modified chitosan generally has multiple functional groups such as amino groups, hydroxyl groups, carboxyl groups and thiols.[44] Upon hydrogen bonding these groups form cage-like chelates, which may complex metal ions.[45] The adsorption process

[a] *D. Zhang, B. Rhimi, C. Wang*
School of Environmental Science and Engineering, Shaanxi University of Science and Technology, Xi'an 710021, P.R. China
E-mail: wangchuanyi@sust.edu.cn
[b] *G. Crini*
Laboratoire Chrono-environnement, UMR 6249, UFR Sciences et Techniques, Université Bourgogne Franche-Comté, 16 route de Gray, 25000 Besançon, France
[c] *E. Lichtfouse*
Aix-Marseille Univ, CNRS, IRD, INRAE, Coll France, CEREGE, Avenue Louis Philibert, 13100 Aix en Provence, France
[d] *E. Lichtfouse*
State Key Laboratory of Multiphase Flow in Power Engineering, Xi'an Jiaotong University, Xi'an, Shaanxi,710049, P.R. China

Supporting information for this article is available on the WWW under https://doi.org/10.1002/tcr.202000073

starts by diffusion of metal ions to adsorbents followed by surface reactions. Chitosan/metal ions complexes are then formed on the surface of the adsorbent following electrostatic attraction and chemical chelation.[46,47] The high adsorption performance of chitosan is explained by the occurrence of multi-functional groups at the chitosan surface.[48]

Chitosan derivatives have recently gained research interest for the treatment of wastewater contaminated by metals and metalloids.[20,49] Comparison of chitosan-based adsorbents and other solid adsorbents shows that chitosan-based adsorbents have usually higher adsorption capacities (Table 1). Here we review the properties, adsorption mechanisms and applications of chitosan for the removal of mercury ions.

2. Physicochemical Properties of Chitosan

Chitosan, poly [(1, 4)-β-2amino-2-deoxy-D-glucose] (Figure 1), is a biodegradable polymer obtained by deacetylation of chitin, one of the most abundant and renewable materials on earth.[57] Chitin and chitosan differ by their degree of deacetylation and solubility in dilute acidic media. In chitin, acetylated units are dominant. When deacetylation of chitin is higher than 40–50 %, chitin becomes soluble in acidic solutions such as dilute acetic acid.[58] Specifically, dissolution is induced at the C_2 position of D-glucosamine units by protonation of amino groups, yet the solubility is also influenced by the distribution of acetyl groups on the chain.[59] Although the main polymeric chain of chitosan is composed of

Dan Zhang received her BS degree in Light Industry Technology and Engineering from Shaanxi University of Science & Technology in 2016. At present, she is pursuing her PhD degree at Shaanxi University of Science & Technology under the supervision of Prof. Chuanyi Wang. Her current research focuses on environmental functional materials for the removal of heavy metal ions from aqueous system.

Grégorio Crini is an environmental polymerist at the Université de Bourgogne Franche-Comté, Besançon, France. His research focus on the environmental aspects of polysaccharide chemistry. He has published more than 200 papers and is a highly cited researcher with h-index of 36 and 11000+ citations. Information: https://chrono-environnement.univ-fcomte.fr/personnes/annuaire/article/crini-gregorio

Eric Lichtfouse is professor of environmental chemistry and scientific writing at Aix-Marseille University and Xi'an Jiaotong University. He has invented carbon-13 dating, which allows to distinguish temporal pools of organic substances in complex media. His research interests include climate, C cycling and pollution. He is chief editor and founder of the journal Environmental Chemistry Letters. He got the Analytical Chemistry Prize from the French Chemical Society and a Journal Citation Award by the Essential Science Indicators. Information: https://cv.archives-ouvertes.fr/eric-lichtfouse

Baker Rhimi is a postdoctoral fellow in the School of Environmental Science and Engineering at Shaanxi University of Science and Technology, China. He received his PhD degree in Chemistry at the University of Tunis El Manar in 2017. His research interest includes synthesis of single-site and nano-confined photocatalysts in porous materials for environmental applications.

Chuanyi Wang is a distinguished professor at Shaanxi University of Science & Technology (SUST), China. Before moving to SUST in 2017, he was a distinguished professor of the Chinese Academy of Sciences (CAS), serving as Director of the Laboratory of Environmental Science & Technology of the Xinjiang Technical Institute of Physics & Chemistry, CAS (2010-2017). He obtained his Ph.D. degree from the Institute of Photographic Chemistry of CAS in 1998, worked in Germany as an Alexander von Humboldt research fellow from 1999 to 2000, and then worked at Tufts University and Missouri University-Kansas City as a research faculty from 2000 to 2010. Currently, Dr. Wang also serves as an associate editor or board member for several international journals. His research interest covers eco-materials and environmental photocatalysis. He has published over 190 papers in peer reviewed journals.

Table 1. The differences between some chitosan-based adsorbents and other reported solid adsorbents for Hg(II) ions adsorption.

Adsorbent	Qe (mg/g)	Physical form	Characterization	pH	Kinetics	Time point/min	Ref
Sulfur rich microporous polymer	595.2	solid	SEM, TEM, BET,	1	PSO	3	50
Porous inorganic materials (ZrOx, ZrOxyPhos and ZrSulf)	514	powder	SEM, EDX, XRD, FTIR, BET, XPS, TGA	6.8	Nonlinear regression analysis	60	51
Fe_3O_4-nanocellulose compounds	149.4	nanocellulose	SEM, TEM, XPS, PSD, XRD, FTIR, DFT	7	Fractal-like mixed 1,2 order	90	52
Functionalized layered double hydroxide	625	gelatinous precipitate	XRD, FTIR, TEM, BET	>2	PSO	80	53
Guanyl-modified cellulose	48	fiber	SEM, FTIR, TGA	6	PSO	100	54
Hydrazide-micro-magnetite chitosan derivative	365.1	particle	FTIR, XPS, TGA, EDX, SEM	5	PFO	30	55
Chitosan/cellulose biocomposite sponge	495	sponge	FTIR, XPS, TGA, SEM, NMR	5.5	PSO	2	21
Hyperbranched polyethylenimine functionalized carboxymethyl chitosan composite adsorbent	1594	particle	FTIR, XPS, TGA, SEM, BET	5.5	PSO	5	20
Amido-functionalized carboxymethyl chitosan/montmorillonite composite	1875	solid	SEM, TEM, XRD, FTIR, XPS	5.5	PSO	5	56
Polyethyleneimine functionalized chitosan-lignin composite sponge	663.5	sponge	SEM, FT-IR, XPS, DTG	5.5	PSO	1	44

Qe stands for the maximum adsorption capacity. Time point represents the steep-sloped portion of the instantaneous adsorption stage. SEM: scanning electron microscopy, TEM: transmission electron microscopy, BET: Brunauer-Emmett-Teller, EDX: energy-dispersive X-ray, XRD: X-ray diffraction, FTIR: Fourier-transform infrared, XPS: X-ray photoelectron spectroscopy, TGA: thermogravimetric analysis, DFT: Density Functional Theory, NMR: Nuclear Magnetic Resonance, DTG: derivative thermogravimetry, PFO: Pseudo-first order kinetics, PSO: Pseudo-second order kinetics.

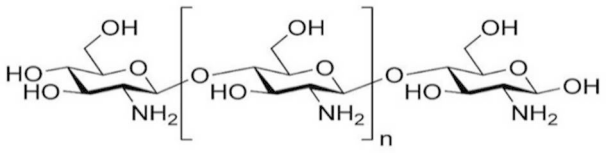

Figure 1. Schematic representation of completely deacetylated chitosan. Chitosan is a biological macromolecule obtained by deacetylation of chitin. Chitosan contains a large number of amino and hydroxyl groups.

hydrophilic functional groups, chitosan is globally hydrophobic.[60] As a consequence, chitosan is usually insoluble both in water at neutral pH and in organic solvents such as dimethylsulfoxide, dimethylformamide, methylpyrrolidone, organic alcohols and pyridine.

The chitosan molecular chain contains many free amino ($–NH_2$), hydroxyl (–OH), *n*-acetyl ($–NH–CO–CH_3$) and other reactive functional groups.[61] These groups are arranged in a regular manner on the molecular chains of the chitosan matrix, thus forming cage molecules which can chelate compounds by hydrogen binding. As a consequence, chitosan forms stable complexes with almost all transition metal ions.[62] Nonetheless, raw chitosan displays some limitations for the remediation of wastewaters contaminated by heavy metals, such as poor selectivity, low adsorption capacity, short pH range, and rather low number of functional groups. Therefore, chitosan has often been chemically modified for application of heavy metal removal.

2.1. Mechanism of Chitosan Adsorption

Adsorption of metal ions on chitosan and chitosan composites occurs by either single or mixed interactions. Metal ions are fixed to amino groups by chelation or coordination.[63] Protonated amino groups and metal cations form complexes under electrostatic attraction in acidic media, then through ion exchange with the protonated amino groups, and the metal cation is steadily adsorbed on the adsorbent.[64] Noteworthy, various interactions can take place simultaneously. The excellent adsorption of heavy metals by chitosan is usually attributed to the large number of hydroxyl groups and amino groups in the molecular chain, the high chemical reactivity of functional groups, the flexible structure of polymer chain, and the strong hydrophilicity.[65–67]

2.2. Modification of Chitosan

Raw chitosan commonly displays low stability in acidic media and weak mechanical strength, which are thus not suitable for industrial applications. Moreover, raw chitosan does not have the ability to selectively adsorb a targeted metal ion in complex wastewater. Therefore, the chemical and mechanical properties of chitosan should be improved by chemical or physical modification.

The adsorption efficiency can be tuned by the surface area, porosity and particle size of the adsorbent.[68] For instance, chitosan flakes and powders are commonly not good for adsorption because of their small surface area and absence of porosity.[69] Alternatively, transformation of chitosan into gels and beads notably improves the adsorption efficiency. This is understandable in view of the expansion of the polymer network, which allows diffusion of metal ions towards internal adsorption sites.[35,70,71] The most common method to prepare chitosan beads and gels is solvent evaporation. Solvent evaporation may also be used to produce chitosan films and fibers.[72] A porous sponge has also be prepared by freeze-drying, during which the chitosan solution or gel is frozen then lyophilized.[21,44]

Chemical modification of chitosan, such as crosslinking and grafting, does not alter the core skeleton of chitosan, but generates new properties allowing higher adsorption capacity and efficiency.[73,74] Many chitosan derivatives have been synthesized by grafting new functional groups on the chitosan backbone to adsorb metal ions.[75] The added functional groups increase the density of adsorption sites, change the pH range of metal ions adsorption and improve the adsorption selectivity.[76] Chemical modification mainly aims at improving the adsorption of metal ions and to change the solubility of chitosan in water or acidic media.[77,78] The substitution reaction involves $–NH_2$ groups at the C_2 position or –OH groups at the C_3 and C_6 positions in acetylated and deacetylated units. Grafts are formed by binding molecules covalently to the chitosan backbone.[79]

Noteworthy, pH is a major factor influencing water treatment by chitosan derivatives.[80] For instance, amino groups are easily ionized at low pH and thus attract anionic pollutants by electrostatic interaction. However, lowering the pH below 5 makes the chitosan gelatinous, which severely limits practical applications.[10] As a result, crosslinking has been used to strengthen the stability of chitosan in acidic media, and also to improve the adsorption performance in terms of capacity and selectivity.[81]

During the crosslinking reaction, an intermediate is formed first with chitosan and the crosslinking agent, and then the new network is stabilized under specific conditions, thus increasing mechanical and chemical stability under acidic conditions.[82] A crosslinking agent is usually a substance containing various functional groups. The agent can be shaped into various forms such as rings, straight chains and branched chains.[83] Common cross-linkers include glutaraldehyde, epichlorohydrin, tripolyphosphate, carboxylic acids and isocyanates.[17,84,85] In particular, epichlorohydrin has the advantage that it does not eliminate the cationic amine function of chitosan, which is the major adsorption site for

metal ions. In general, higher cross-linking decreases the number of free amino groups, the number of reaction sites and therefore the adsorption capacity.[86] Nonetheless, the adsorption capacity may be enhanced by using different types of functional groups in the crosslinking agent. Overall, the stability and mechanical properties of chitosan are improved after crosslinking.

3. Preparation and Characterization of Chitosan-based Composite Adsorbents

3.1. Chitosan-cellulose Biocomposite Sponge

A chitosan/cellulose biocomposite sponge is prepared by mixing solutions of chitosan and polyvinyl alcohol, then a cellulose suspension is added. After 3 hours of stirring, glutaraldehyde is added dropwise under stirring to yield a yellow sol, which is then frozen and lyophilized.[21]

The C and N composition on the surfaces of chitosan and the chitosan/cellulose biocomposite sponge can be analyzed by X-ray photoelectron spectroscopy (XPS, Figures 2a and 2b). The N 1s spectrum of the biocomposite displays two peaks, and the N 1s (399.36)/N 1s (401.71) ratio is weaker than that of chitosan,[87] indicating that some amino groups were involved in a Schiff base reaction with glutaraldehyde. Compared to chitosan, the broad peaks of C1s of the biocomposite at 284.78 eV, 286.36 eV, 287.9 eV and 288.87 eV correspond to sp1 (C–C), bonded carbon (C–O), imine bond (C=N), and amide bond, respectively. These results confirm the successful Schiff base reaction.

Analysis by nuclear magnetic resonance (NMR) shows that the biocomposite is globally similar to the unmodified biopolymer (Figure 2c). For instance, ^{13}C shifts of C_1 at 105.8 ppm, C_2 at 57.7 ppm, $C_{3,\ 5}$ at 76.2 ppm, C_4 at 83.3 ppm, C_6 at 62.0 ppm and CH_3 at 24.2 ppm indicate that the biocomposite has a similar structure as the chitosan precursor.[88] Nonetheless, the biocomposite shows new peaks, which can be attributed to conjugated ethylene bonds at 100.1 ppm and 129.5 ppm, and imine bonds at 179 ppm.

The Fourier transform infrared (FTIR) spectra of cellulose, chitosan, and chitosan/cellulose biocomposite sponge are shown in Figure 2d. The absorption peaks at 3405 cm^{-1}, 2899 cm^{-1}, 1431 cm^{-1}, and 1059 cm^{-1} are attributed to –OH, C–H, $–CH_2$, C–O–C stretching of cellulose, respectively. For chitosan, the peaks at 3350–3450 cm^{-1} correspond to –OH and –NH stretched vibrations, respectively. The vibration peaks of 1653 cm^{-1} and 1558 cm^{-1} are due to amide I and amide II.[89] The peak at 3344 cm^{-1} of the chitosan/cellulose biocomposite sponge is ascribed to –OH and $–NH_2$ stretching. In addition, the absorption peak at 1638 cm^{-1} is attributed to the C=O stretching of amide I.[90] The C=N band is formed by the cross-linking of chitosan and glutaraldehyde and also appears in this region, which further proves the effective Schiff base reaction.

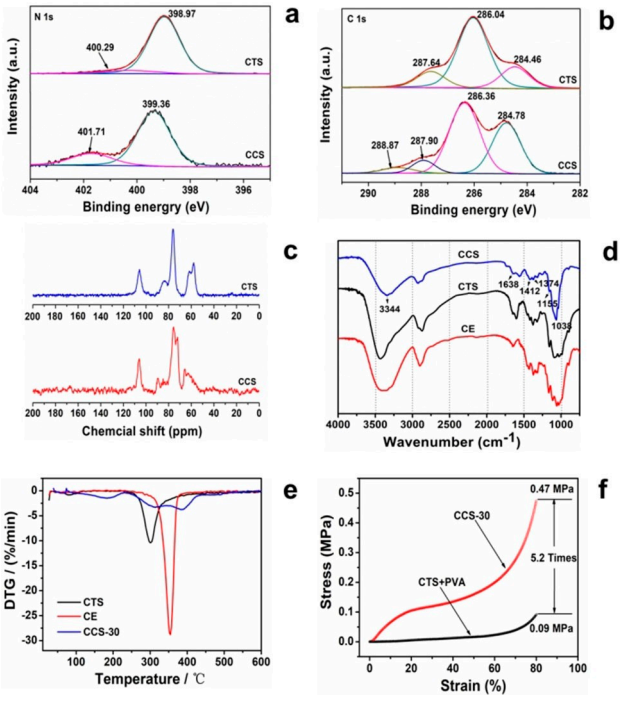

Figure 2. a) High-resolution N 1s spectra; the N 1s (399.36)/N 1s (401.71) of the chitosan/cellulose sponge (CCS) is weaker than that of chitosan (CTS), indicating that some amino groups reacted with glutaraldehyde. b) C 1s of spectra from XPS analysis; compared to chitosan the broad peaks of C1s of chitosan/cellulose sponge at 287.9 eV correspond to imine bonds C=N. c) ^{13}C solid-state NMR spectra of chitosan/cellulose sponge and chitosan are very similar, new peaks at 100.1 ppm and 129.5 ppm can be attributed to conjugated ethylene bonds, and imine bonds at 179 ppm. d) Fourier transform infrared spectroscopy show that the peak at 1638 cm^{-1} is due to C=O stretching of amide I; the C=N bond band formed by crosslinking chitosan and glutaraldehyde also appear in this region, thus proving the Schiff base reaction. e) Derivative thermogravimetric (DTG) curves: the mass loss differences of chitosan, cellulose (CE), and chitosan/cellulose sponge indicate that the crosslinking was successful. f) Compressive stress-strain curves show that under 80% strain the cross-linking of chitosan improved the mechanical strength of the material and the compressive strength. PVA: polyvinyl alcohol.[21] Copyright © 2019 Elsevier B.V.

The thermal stability of chitosan and chitosan/cellulose biocomposite sponge was analyzed by thermogravimetry (Figure 2e). The slight mass loss at about 100 °C is due to the evaporation of adsorbed water. Compared with chitosan and cellulose, the biocomposite shows thermal events at 183 °C, 314 °C and 389 °C, which could be explained by the decomposition of junctions between cellulose and chitosan.[91] This observation also indicates that glutaraldehyde participates in the cross-linking reaction, and that the thermal stability is enhanced.

Mechanical properties of the material are essential for practical applications. As seen from Figure 2f (red curve), the

chitosan/cellulose biocomposite sponge has good mechanical properties, but the compression modulus is reduced due to the weakening of hydrogen bonding within polymers, as a consequence of glutaraldehyde cross-linking.[92] The mechanical strength of the strain-hardened zone is further enhanced because of the coating of the chitosan in the porous structure, which in turn increases the compressive strength.

3.2. Polyethyleneimine-functionalized Chitosan-lignin Composite Sponge

For the preparation of polyethyleneimine functionalized chitosan–lignin composite sponge, the protocol for preparing chitosan/cellulose biocomposite sponge can be adopted.[21] Polyethyleneimine is added after the chitosan and polyvinyl alcohol are mixed, then the mixture is mechanically stirred.[44] Figures 3a and 3b show the digital and microscopic photos of the composite sponge, highlighting that the sponge has an uneven and dense porous structure. The scanning electron microscope (SEM) image further proves that the composite sponge has an interconnected porous structure. The experimental data in Figure 3c shows a nanosheet thickness of about 75 nm, which is intertwined to form a thin wall.[93]

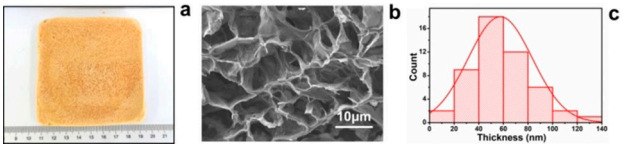

Figure 3. a) Digital photo and b) Scanning electron microscope (SEM) images of the polyethyleneimine chitosan-lignin sponge (PEI–CS–L). The micrograph shows that the composite sponge has interconnected porous structures. c) Normal distribution of nanowalls thickness, showing a nanosheet thickness of about 75 nm, which is intertwined to form a thin wall.[44] Copyright © 2020 Royal Society of Chemistry.

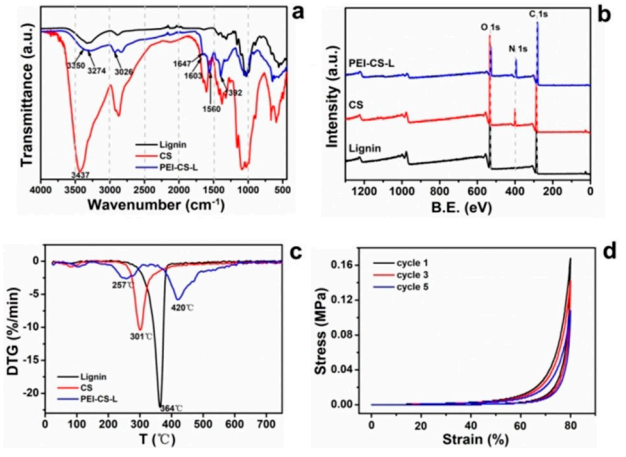

Figure 4. a) Fourier transform infrared spectra (FT-IR), and b) X-ray photoelectron spectra (XPS) of the polyethyleneimine functionalized chitosan-lignin (PEI–CS–L) sponge, confirming that glutaraldehyde has well cross-linked chitosan and polyethyleneimine. c) Derivative thermogravimetry (DTG) curves of lignin, chitosan (CS) and the PEI–CS–L sponge, further demonstrating the successful preparation of the composite sponge. d) Compressive stress-strain curves of the PEI–CS–L sponge after different cycles, showing that the sponge keeps a stable three-dimensional network structure.[44] Copyright © 2020 Royal Society of Chemistry.

Figure 4a compares the infrared spectra (FT-IR) of the synthesized sponge with chitosan and lignin precursors. Here the sponge shows strong N–H stretching peaks at 1392 cm^{-1} and 1560 cm^{-1}.[94] These two peaks are attributed to primary amines and secondary amines, respectively. In addition, the sponge has a characteristic peak caused by C=N stretching at about 1647 cm^{-1}, which indicates that glutaraldehyde is an efficient cross-linker of chitosan and polyethyleneimine. In the X-ray photoelectron spectroscopy (XPS) spectrum (Figure 4b), the signal intensity of N in the sponge is significantly higher than that of the other two precursors, which suggests the successful introduction of polyethyleneimine.[95]

Figure 4c shows the differential thermogravimetric (DTG) analysis of the synthesized sponge and two precursors. At 364 °C, lignin displays an endothermic peak due to the cleavage of hydrogen-oxygen bonds, which are abundant in lignin. The heat loss of chitosan at 301 °C is related to the rupture of the main chain, and to the release of some small molecular fragments.[96] The thermal decomposition temperature of the composite sponge at 420 °C is higher than that of the two precursors, which demonstrates the successful formation of the composite. The endothermic peak at 257 °C is attributed to the thermal decomposition of polyvinyl alcohol in the composite sponge.[97] Figure 4d shows the compressive stress-strain curve of the composite sponge. Results show that the original sponge has a full elasticity and can recover nearly 100 % deformation after stress release.[98] The stress-strain curve of the sponge does not change significantly after different cycles, which implies that the sponge is rather stable.

3.3. Hyperbranched Polyethylenimine-functionalized Carboxymethyl Chitosan Composite

Hyperbranched polyethylenimine-functionalized carboxymethyl chitosan composite (HPFC) can be synthesized in one-step. First, a certain proportion of carboxymethyl chitosan, polyethylenimine, and polyvinyl alcohol are dissolved in ultrapure water, and then glutaraldehyde solution of a certain quality is added. After 30 minutes, the mixture is stirred at room temperature for 6 h until the Schiff base reaction is complete, yielding a pink flocculent precipitate. After filtration, the solid is washed with deionized water several times, and then lyophilized.

Figures 5a and 5b show the adsorption-desorption curve and pore size distribution of the carboxymethyl chitosan and HPFC composite, using N_2 adsorption isotherms. The results

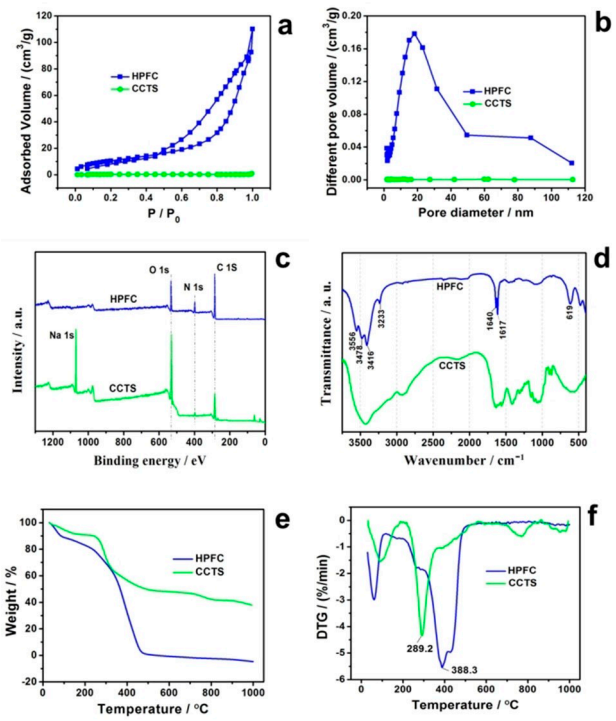

Figure 5. (a) Adsorption-desorption curves, and (b) Pore diameter distributions indicate the presence of mesopores; and the increase of the total pore volume reveals the porous structure of the synthesized hyperbranched polyethylenimine functionalized carboxymethyl chitosan composite (HPFC). c) XPS spectra and d) FT-IR spectra, showing that the crosslinking reaction of carboxymethyl chitosan (CCTS), polyethylenimine (PEI), and glutaraldehyde (GLA) was successful. e) TGA and f) DTG, supporting that the crosslinking between PEI and CCTS enhances the thermal stability.[20] Copyright © 2019 Elsevier B.V.

clearly show that the two samples exhibited typical type-IV S-type curve. The pore diameter distribution curves were drawn using Barrett-Joyner-Halenda (BJH) analysis, and the average pore size of HPFC was 11.9 nm, indicating the presence of mesopores.[99] The total pore volume of HPFC was found to be 8.1×10^{-2} cm^3/g, which is 62 times that of CCTS. Compared with carboxymethyl chitosan, HPFC has a higher specific surface area of 22.3 m2/g and total pore volume of 8.1×10^{-2} cm^3/g (Table S1). This higher pore volume and specific surface area confer HPFC a porous structure, which is beneficial for the removal of Hg(II) ions.

X-ray photoelectron spectroscopy (XPS) in Figure 5c shows that the N signal of the HPFC composite is stronger than that of the carboxymethyl chitosan precursor, indicating that polyethylenimine was effectively introduced.[100] Fourier transform infrared spectroscopy (FT-IR) shows the differences between carboxymethyl chitosan and HPFC (Figure 5d). The stretching vibration of O–H shows strong peaks at ~3556 cm^{-1}; the peaks at 3478 cm^{-1}, 3416 cm^{-1} and 3233 cm^{-1} are due to N–H for primary and secondary amines;[101] and the peak at 1617 cm^{-1} also illustrates the presence of N–H. The peak at 1640 cm^{-1} is attributed to the C=N bond,[102,103] which indicates the successful grafting of polyethylenimine onto carboxymethyl chitosan by glutaraldehyde during the Schiff base reaction.

The thermal properties of carboxymethyl chitosan and composites were generally evaluated using thermogravimetric analysis (TGA) and derivative thermogravimetric analysis (DTG). Figures 5e and 5f show two major degradation stages. The weight loss around 100 °C is considered as water evaporation. The major thermal loss of the composite is caused by the backbone decomposition at 388.3 °C, which is much higher than that of carboxymethyl chitosan.[104]

3.4. Amido-functionalized Carboxymethyl Chitosan/Montmorillonite Composites

HPFC/Montmorillonite-S adsorbent was prepared by adding mercaptopropyl modified montmorillonite.[20] First, the modified montmorillonite is sonicated in deionized water, and then carboxymethyl chitosan, polyethyleneimine, and polyvinyl alcohol are added sequentially, followed by stirring. The subsequent steps are equivalent to the previous system. The obtained samples were named HPFC/x% Montmorillonite-S, where x% represents the percentage of montmorillonite-S in the HPFC.[56]

X-Ray diffraction (XRD) patterns of sulfhydryl-modified montmorillonite and various composite materials are shown in Figure S1a. The characteristic diffraction peaks are located at 66.06°, 19.81°, 20.75°, 26.61°, and 61.72°. The diffraction peak intensity of the HPFC/Montmorillonite-S composites decreases after addition of Montmorillonite-S.[105] Nonetheless, when the matrix content of Montmorillonite-S is lower than 15%, no clear diffraction peak is observed for Montmorillonite-S, because Montmorillonite-S nanosheets are uniformly dispersed. When the content of Montmorillonite-S is higher than 15%, the intensity of these typical diffraction peaks increases with Montmorillonite-S content, but the position does not change significantly. These findings imply that a large number of Montmorillonite-S particles occur as aggregates in the polymer matrix, and that the organic polymer does not change the crystal structure of Montmorillonite-S.[106–108] In addition, Fourier transform infrared spectroscopy (FT-IR) and X-ray photoelectron spectroscopy (XPS) analyses of the Montmorillonite-S and HPFC/Montmorillonite-S composites are shown in Supporting Information (Figures S1b–g).

4. Adsorption Properties and Mechanism of Chitosan-based Composite for Hg(II) Ions

4.1. Adsorption Properties

Zhang et al.[44] synthesized a polyethyleneimine functionalized chitosan-lignin composite sponge to test the adsorption of Hg (II) ions in aqueous solution. In order to avoid the precipitation of Hg(II) ions, adsorption studies were performed from pH 1.5 to 5.5 to assess the effect of pH on removal of Hg(II) ions.

Figure 6 shows the relationship between pH and the adsorption capacity. The adsorption capacity increases with pH, reaching a maximum adsorption capacity of 663.5 mg/g at 5.5. This is explained by the lower protonation of amino groups at high pH, which favors Hg(II) ions binding. The adsorption of Hg(II) ions is mainly driven by chelation with the active sites.

The adsorption kinetics of Hg(II) ions by the polyethyleneimine functionalized chitosan–lignin composite sponge is shown in Figures 7a and 7b. Results show that the adsorbent completes 83.5 % of the total adsorption in 1 minute, and reaches equilibrium in 6 hours at 663.5 mg/g. The good adsorption performance is attributed to the porous structure containing nanoscale interconnected walls, and to the large number of active sites for Hg(II) ions adsorption. Three kinetic models were used to describe the entire adsorption process, and correlation coefficients are shown in Table S2. The highest correlation with R^2 of 0.99 was obtained for the pseudo-second-order model, indicating that the adsorption of Hg(II) ions by the composite sponge is the nature of chemical adsorption.

The adsorption capacity of the composite sponge for Hg (II) ions increases with initial Hg concentration until reaching saturation (Figures 7c and 7d). This is explained by the increasing number of Hg(II) ions in the solution, which in turn favors collisions with sponge active sites. According to the correlation coefficient value (Table S3), the Langmuir model with R^2 of 0.99 describes better the adsorption process than the Freundlich model. Here, the theoretical maximum adsorption value is close to the experimental value, indicating that the reaction involves single layer adsorption. The thermodynamic properties of the polyethyleneimine functionalized chitosan-lignin composite sponge complex were tested at 293, 303 and 313 K (Figure 7e, Table S4). The Gibbs free-energy (ΔG, kJ mol^{-1}) increases with increasing temperature, showing that the adsorption of Hg(II) ions is spontaneous whatever the temperature.

The properties of the composite sponge were compared with those of other lignin-based adsorbents in terms of adsorption capacity, response time and adsorption efficiency (Table 2). Results show that the composite sponge removes 83.5 % of the total adsorption capacity within 1 minute, which is much faster than most others.

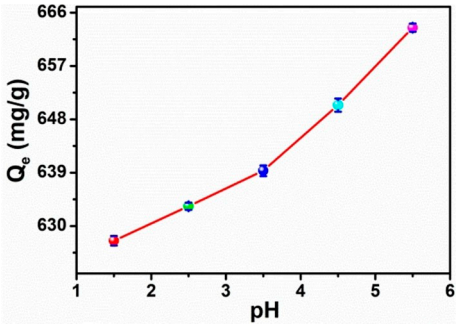

Figure 6. Effect of pH on the adsorption capacity of the polyethyleneimine functionalized chitosan–lignin composite sponge (PEI–CS–L) for Hg(II) ions, showing that the adsorption capacity of Hg(II) increases with pH. Adsorption experiments – C_0 664.1 mg/L, sample dose 25 mg/25 mL, pH range 1.5–5.5; temperature 30 °C, adsorption time 6 h.[44] Copyright © 2020 Royal Society of Chemistry.

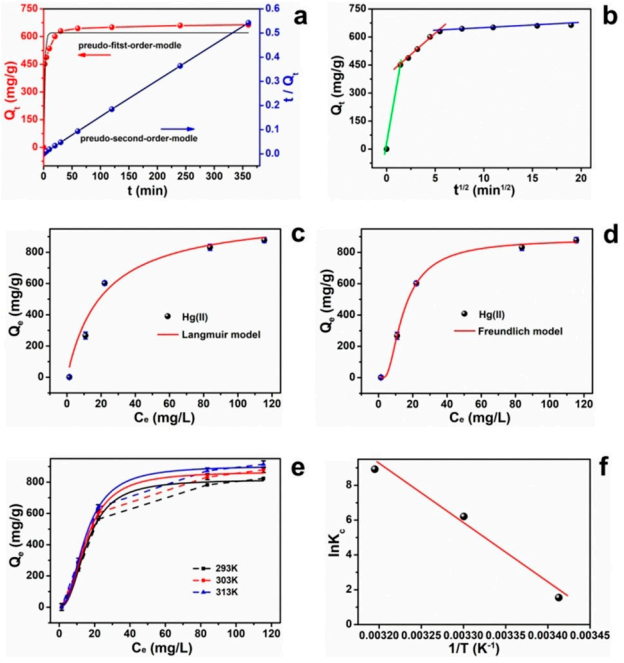

Figure 7. a) Pseudo-first order, pseudo-second order, and b) intra-particle diffusion models, showing that adsorption reaches 83.5 % of the initial adsorption amount in 1 min, and reaches equilibrium in 6 hours at 663.5 mg/g. c) Langmuir and d) Freundlich model, demonstrating that the Langmuir model better describes the adsorption process, and that the adsorption proceeds by a single layer. e) Effect of temperature on the adsorption and f) lnK_c versus 1/T for Hg(II) ions by the polyethyleneimine functionalized chitosan-lignin composite sponge, indicating the adsorption process is spontaneous and feasible. (C_0 1–1000 mg/L, sample dosage 25 mg/25 mL, temperature 20, 30, 40 °C, pH 5.5, contact time 1–360 min).[44] Copyright © 2020 Royal Society of Chemistry.

Table 2. Comparison of equilibrium adsorption time, adsorption capacity, ultimate equilibrium adsorption capacity, and equilibrium percentage of ultimate adsorption capacity of a polyethyleneimine functionalized chitosan–lignin composite (PEI–CS–L) sponge with various lignin-based adsorbents for heavy metal ions.[44] Copyright © 2020 Royal Society of Chemistry.

Adsorbent	Heavy metal ions	t (min)	q_t (mg/g)	q_m (mg/g)	E (%)	Ref
Porous lignin based poly (acrylic acid)/organo-montmorillonite nanocomposites	Pb(II)	30	128.9	223.78	57.6	[109]
Sodium lignosulphonate assisted synthesis of Fe_3O_4 microspheres	Cu(II)	60	45	75	60	[110]
TiO_2–SiO_2/lignin hybrids	Pb(II)	28	11.7	12.7	92	[111]
5-sulfosalicylic acid modified lignin	Pb(II)	12	27.9	39.3	71	[112]
Poly(ethylene imine) anchored lignin composite	Cu(II)	5	49	98	50	[113]
PEI–CS–L	Hg(II)	1	554	663.5	83.5	[44]

Marks: t, q_t, and q_m stand for the time of approaching equilibrium, the adsorption capacity of approaching equilibrium, and the adsorption capacity at equilibrium; E represents xx % of the total removal that can be achieved in t minute. PEI–CS–L: polyethyleneimine functionalized chitosan–lignin composite sponge.[44]

Zeng et al.[20] prepared hyperbranched polyethylenimine functionalized carboxymethyl chitosan composite (HPFC) to adsorb Hg(II) ions in aqueous solutions. Figure 8a shows that 80 % of initial Hg(II) ions are adsorbed by the HPFC composite in 5 min. After 12 hours, nearly 100 % of Hg(II) ions are removed, with a final Hg aqueous concentration of 0.02 mg/L, which is lower than the national industrial wastewater discharge standard of 0.05 mg/L. Such super efficiency is attributed to numerous pores and adsorption sites on the developed composite adsorbent.

In order to understand the adsorption process, three kinetic models were fitted to the experimental data (Figure 8b and c). Results show that the correlation of the pseudo second-order model with R^2 of 0.99 is better than that of the pseudo first-order model, and the fitted Q_f value is very close to the experimental value (Table S5). This means that interactions between materials and Hg(II) ions proceed by chemical binding. For instance, according to the theory of hard and soft acids and bases, heavy metal ions such as Hg^{2+}, Hg_2^{2+}, Pd^{2+}, Ag^+ and Au^+ are soft Lewis acids, which can easily interact with soft Lewis bases such as amine/imine, carboxyl and sulfhydryl groups through coordination bonds. Nonetheless, the particle diffusion model also describes well the adsorption process. In summary, the adsorption process of Hg(II) ions by HPFC is complicated, involving intra-particle diffusion and chemical adsorption.

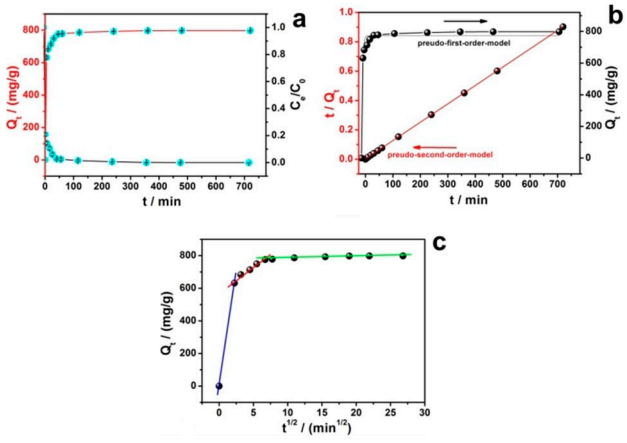

Figure 8. a) Effect of contact time on Hg(II) adsorption by the hyperbranched polyethylenimine-functionalized carboxymethyl chitosan composite (HPFC), showing that nearly 100 % of Hg(II) ions were removed after 720 min. b) Pseudo-first order, pseudo-second order and c) Intra-particle diffusion model, suggesting that the adsorption of Hg(II) ions on HPFC is well described by the pseudo-second order model. C_0 798.1 mg/L, sample dosage 20 mg/20 mL, temperature 30 °C, pH 5.5.[20] Copyright © 2019 Elsevier B.V.

Furthermore, Zeng et al.[20] also tested the removal performance of HPFC using a real water sample from a gas field in China. The main components (mg/L) of the real water sample include Hg (8.44), Na (9426), Mg (685), Ca (1624), Cl^- (14574), NO_3^- (155), SO_4^{2-} (68), HCO_3^- (201). 20 mg of dried HPFC was immersed into 20 mL of water and stirred at room temperature for 24 h. After filtration, the concentration of the solution was measured by atomic fluorescence spectrophotometer (AFS). Results show that HPFC decreases the Hg(II) ions concentration to 0.15 mg/L with a removal efficiency of 98.2 %. Thus, HPFC has good potential in practical applications.

The effects of the adsorbent on the adsorption capacity of Hg(II) ions at different temperatures were studied (Figures 9a and 9b). The results are shown in the Supporting Information. Figure 9c shows the adsorption capacity versus initial Hg(II) concentration. The curves show an increase followed by a plateau. Langmuir, Freundlich and Langmuir-Freundlich models were used to fit the adsorption data. Results show that Langmuir-Freundlich adsorption model fits better than the other two models (Table S7). As a consequence, the adsorption of Hg(II) ions proceeds both by single-layer and multi-layer coordinated adsorption.

Table 3. Comparison of Hg(II) ions adsorption on hyperbranched polyethylenimine functionalized carboxymethyl chitosan composite (HPFC) and other adsorbents.[20] Copyright © 2019 Elsevier B.V.

Adsorbent	pH	T (°C)	t_e (min)	Q_e (mg/g)	Q_m (mg/g)	Ref
Ethylenediamine-modified magnetic crosslinked chitosan microspheres	5.0	25	120	407.2	539.6	[117]
Formaldehyde cross-linked modified chitosan	5.0	30	60	85.33	98	[118]
Glutaraldehyde cross-linked chitosan	5.0	25	200	56	145	[70]
Glutaraldehyde cross-linked magnetic chitosan	5.0	25	200	58	152	[119]
Poly(vinyl alcohol)-modified glutaraldehyde crosslinking chitosan	5.5	30	1440	723.87	769.23	[120]
Poly(maleicacid)-grafted crosslinked chitosan	6	30	45	601	1044	[121]
HPFC	5.5	30	360	1584	1594	[20]

The adsorption selectivity of HPFC was tested by single adsorption and mixed adsorption experiments. As shown in Figure 10a, the adsorption capacity of Hg(II) ions by HPFC in the single-component solution can reach 797.47 mg/g, far higher than that of other heavy metal ions. The adsorption capacity of different heavy metal ions follows the order Hg(II) > Pb(II) > Cu(II) > Cd(II), which indicates that HPFC has adsorption selectivity for Hg(II) ions.[114–116] This was further confirmed by mixed ions adsorption. As shown in Figure 10b, HPFC shows a good adsorption capacity for Hg(II) ions even in the mixed component solution, with the adsorption capacity of 318.95 mg/g. The adsorption capacities of Pb(II), Cu(II) and Cd(II) ions were 59.45, 49.37 and 38.42 mg/g, respectively.

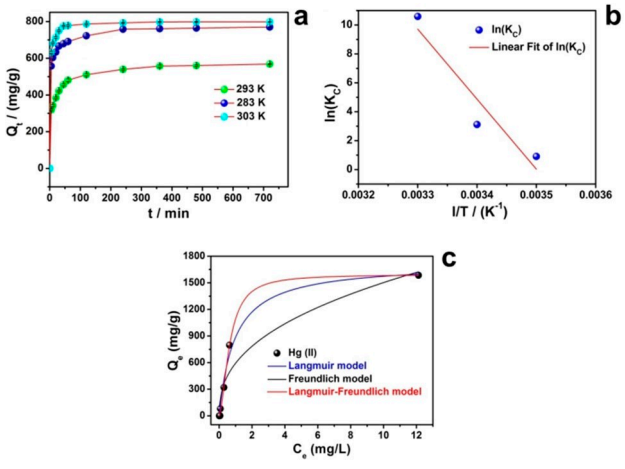

Figure 9. a) Effect of temperature on the adsorption, and b) lnK_c versus 1/T, showing increasing Hg(II) ions adsorption capacity with temperature. c) Adsorption isotherms for Hg(II) ions on the hyperbranched polyethylenimine-functionalized carboxymethyl chitosan composite (HPFC), suggesting that the adsorption behavior is better described by the SIPS model (Langmuir-Freundlich adsorption model) compared to the Langmuir and Freundlich models. Sample dosage 20 mg/20 mL, C_0 10 ~ 798.1 mg/L, temperature 20, 30, 40 °C, pH 5.5, adsorption time 360 min, 720 min.[20] Copyright © 2019 Elsevier B.V.

The HPFC adsorbent has superior adsorption capacity, which can be illustrated by comparison with other reported chitosan-based adsorbents (Table 3). As a result, although the separation performance of HPFC is not as good as that of magnetic materials, the removal efficiency of Hg(II) ions is obviously better than any other known chitosan-based adsorbents. Noteworthy, the simulated Hg(II) ions wastewater treated by HPFC reaches the national industrial wastewater discharge standard, a performance which has been rarely attained so far.

The amido-functionalized carboxymethyl chitosan/ montmorillonite composite prepared by Zeng et al.[56] was also used to adsorb Hg(II) ions in aqueous solutions. Figure S2a shows the trend of removal efficiency and residual concentration with the initial pH value. Here, the adsorption efficiency is higher than 90 % at a pH 1.5. The removal rate first increases and then remains stable with pH. The electrostatic theory shows that at low pH the adsorbent surface bears more positive charges, which prevents the occupation of active sites by metal ions, and, in turn, the amount of adsorption decreases sharply. Increasing the pH of the solution reduces electrostatic repulsive forces due to the release of positive charges, which improves the adsorption efficiency of metal ions. In addition, the adsorption capacity is stable under strong acids. It was found that the chelation between N, O, S groups and Hg(II) ions does not involve electrostatic interactions, but instead of

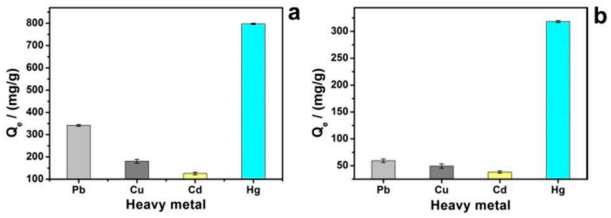

Figure 10. Selective adsorption by hyperbranched polyethylenimine-functionalized carboxymethyl chitosan composite. Sample dosage 20 mg/20 mL, temperature 30 °C, pH 5.5, adsorption time 360 min. a): Single component solution; b): Mixed component solution.[20] Copyright © 2019 Elsevier B.V.

chemisorption. Moreover, after treatment, the final concentration of Hg(II) ions in water at pH 5.5, of 0.031 mg/L, is lower than the industrial emission standard, of 0.05 mg/L.

The adsorption capacity of Hg(II) ions at different contact times is shown in Figure S2b. HPFC/28 % Montmorillonite-S shows a fast adsorption process. In 5 minutes, the adsorption efficiency is higher than 80 %, and then a slower removal occurs until the maximum adsorption reaches 999.97 mg/g. The kinetic mechanism and the thermodynamic adsorption experiment were explored in the Supporting Information.

4.2. Adsorption Mechanism

The mechanism of selective adsorption of different heavy metal ions in aqueous solution on HPFC materials prepared by Zeng et al.[20] was explained by the density functional theory (DFT).[122,123]

The monomer structure of polyethyleneimine-glutaraldehyde-double carboxymethyl chitosan was optimized using the highest occupied molecular orbital (HOMO) and the lowest unoccupied molecular orbital (LUMO).[124,125] Results show that HOMO and LUMO are mainly situated in nitrogen groups (–NH_2, –C=N) and oxygen groups (–COO–), which are thus the preferred sites for heavy metal ions adsorption. The optimized structure of the complex of polyethyleneimine-glutaraldehyde-double carboxymethyl chitosan monomer and metal ions is shown in Figure 11. Table 4 also shows the binding energies (E_{ad}) of various complexes. Results show that the larger the absolute value of the binding energy, the stronger interaction force between the adsorbent and metal ions. For Hg(II) ions, the maximum adsorption value of E_{ad} confirms the synergistic effect of N groups (–NH_2, –C=N) and O group (–COO–) for strong chelation.

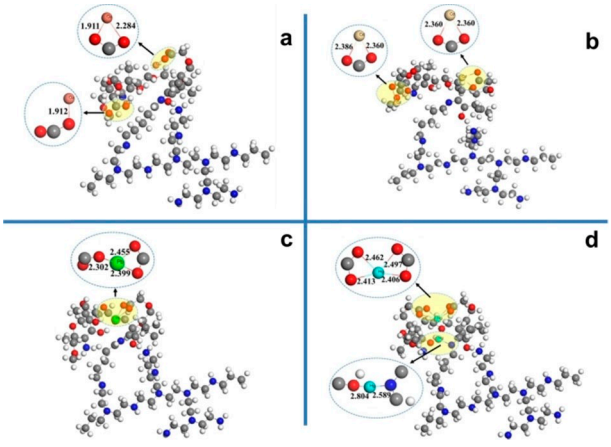

Figure 11. Optimized structure of polyethylenimine-glutaraldehyde-double carboxymethyl chitosan monomer with a) Cu, b) Cd, c) Pb and d) Hg, indicating that amino (–NH_2, –C=N) and oxygen groups (–COO–) are the main functional groups for the adsorption of heavy metal ions, and the more negative the adsorption energy value is, the stronger is the interaction between the metal-adsorbent complex. The H, C, N, and O are depicted by white, grey, blue, and red, respectively.[20] Copyrights © 2019 Elsevier B.V.

The mechanism of the interaction between Hg(II) ions and the adsorbent prepared by Zeng et al.[51] was studied by XPS and EDS-Mapping. Results show that O, N and S groups of HPFC/28 % Montmorillonite-S were involved in the adsorption process of Hg(II) ions. Hg(II) ions exist in the form of Hg^{2+}, $HgOH^+$, and $Hg(OH)_2$ in the aqueous solution according to the pH value. Free Hg^{2+} mainly exists below pH 4, $HgOH^+$ and $Hg(OH)_2$ coexist at pH value 4 ~ 6, and $Hg(OH)_2$ predominates above pH 6. The involved complexation reaction can be described by:

$$\equiv C{-}NH + Hg^{2+} + 2NO_3^- \rightarrow \equiv C{-}N{-}Hg^{2+},\ NO_3^- + HNO_3 \quad (1)$$

$$\equiv C{-}NH + HgOH^+ + NO_3^- \rightarrow \equiv C{-}N{-}HgOH + HNO_3 \quad (2)$$

$$\equiv C{-}NH + Hg(OH)_2 \rightarrow \equiv C{-}N{-}HgOH + H_2O \quad (3)$$

The mechanism can be explained as follows: at low pH, Hg(II) ions occurs as Hg^{2+}, which adsorbs onto active groups to form positively charged complexes. These charged complexes form an electrostatic barrier that prevents adsorption. At higher pH, hydroxylated mercury $HgOH^+$ and $Hg(OH)_2$ interacts with reactive groups to form neutral complexes such as N–HgOH. As the adsorption process proceeds, more and more hydroxylated mercury forms chelate and aggregates on

Table 4. Optimized adsorption energies calculated by the density functional theory (DFT) for the interaction of heavy metal ions with polyethyleneimine-glutaraldehyde-double carboxymethyl chitosan monomer.[20] Copyrights © 2019 Elsevier B.V.

Adsorption site	E_{ad}/eV Cu(II)	Cd(II)	Pb(II)	Hg(II)
One ion was adsorbed on the amino binding site	0.85	1.48	0.16	1.51
One ion was adsorbed on the carboxyl binding site	−0.20	0.31	0.48	−0.86
Two ions were adsorbed on the amino binding site	−0.14	−0.66	0.26	**−3.71**
Two ions were adsorbed on the carboxyl binding site	**−1.14**	**−0.93**	**−1.99**	1.08

the active sites. Aggregates gradually grow up due to the interference of hydrogen bonds and foreign particles, producing a heterogeneous solid matter. Overall, the presumed mechanism of Hg(II) ions removal involves not only chelation at the adsorption-solution interface, but also precipitation on the adsorbent surface.

5. Conclusion

How to rationally recycle and utilize Hg(II) ions, and to reduce their harm to the environment and human body is a matter worthy of profound understanding and substantial endeavors. In this review, we have articulated the research progress of chitosan-based and chitosan derivatives-based adsorbents employed for the removal of Hg(II) ions. The use of chitosan and chitosan derivatives for removing Hg(II) ions from contaminated solutions presents many attractive features such as acid and alkali resistance, strong adsorption capacity, rapid kinetic, high selectivity, easy recycling and renewable, etc. Nevertheless, many challenges need to be tackled before the actual application of chitosan-based adsorbents. Environmentally friendly modifying agent and green preparation methods are highly recommended for processing such adsorbents. Although many current modifications could increase the adsorption performance of the adsorbents, organic or inorganic reagents used in the preparation may cause secondary pollution to the environment. Also, the co-adsorption performance in a real case should be considered as an important future research direction. In practice, a large number of organic pollutants and heavy metal ions coexist in wastewater, which poses a greater challenge to the design of corresponding adsorbents. If being able to remove heavy metal ions and organic pollutants simultaneously, it will lead to a wider application of such adsorbents. One-time treatment to reach the emission standards can reduce subsequent treatment costs and reduce secondary pollution, which is a key to environmental remediation. Considering the complexity of heavy metal pollution, an eco-friendly adsorbent with a capacity of completely removing pollutants is urgently desired.

Acknowledgements

This project was supported by the National Nature Science Foundation of China (Grant No. U1403295), and SAFEA of China (High-end foreign expert project # GDT20186100427).

References

[1] Z. Rahman, V. P. Singh, *Environ. Monit. Assess.* **2019**, *191*, 419.
[2] R. B. Jain, *Environ. Res.* **2019**, *169*, 342–347.
[3] N. V. Dolgova, S. Nehzati, T. C. MacDonald, K. L. Summers, A. M. Crawford, P. H. Krone, G. N. George, I. J. Pickering, *Metallomics* **2019**, *11*, 621–631.
[4] Y. Gao, X. R. Huang, H. H. Wang, F. Zhao, Y. H. Li, *Oxid. Commun.* **2016**, *39*, 917–926.
[5] C. Sarin, J. M. Hall, J. Cotter-Howells, K. Killham, M. S. Cresser, *Environ. Toxicol. Chem.* **2000**, *19*, 259–264.
[6] A. Chatterjee, M. Banerjee, D. G. Khandare, R. Gawas, S. C. Mascarenhas, A. Ganguly, R. Gupta, H. Joshi, *Anal. Chem.* **2017**, *89*, 12698–12704.
[7] A. C. Bourtsalas, N. J. Themelis, *Waste Manage.* **2019**, *85*, 90–94.
[8] F. Steenhuisen, S. J. Wilson, *Atmos. Environ.* **2015**, *112*, 167–177.
[9] G. Crini, E. Lichtfouse, L. Wilson, N. Morincrini, *Environ. Chem. Lett.* **2019**, *17*, 195–213.
[10] X. H. Wang, L. Yang, J. P. Zhang, C. Y. Wang, Q. Y. Li, *Chem. Eng. J.* **2014**, *251*, 404–412.
[11] X. Y. Mao, L. Wang, C. Y. Wang, E. Lichtfouse, *Environ. Chem. Lett.* **2018**, *16*, 1429–1434.
[12] Q. Zhang, L. Na, Y. Cao, W. Zhang, Y. Wei, F. Lin, J. Lei, *Appl. Surf. Sci.* **2018**, *434*, 57–62.
[13] G. Guan, S. Y. Zhang, Y. Cai, S. Liu, M. S. Bharathi, M. Low, Y. Yu, J. Xie, Y. Zheng, Y. W. Zhang, *Chem. Commun.* **2014**, *50*, 5703–5705.
[14] C. Jeon, K. H. Park, *Water Res.* **2005**, *39*, 3938–3944.
[15] W. Liu, X. Zhao, T. Wang, J. Fu, J. R. Ni, *J. Mater. Chem.* **2015**, *3*, 17676–17684.
[16] N. Li, R. B. Bai, C. K. Liu, *Langmuir*, **2005**, *21*, 11780–11787.
[17] C. Hou, D. Y. Zhao, S. F. Zhang Y Yang, *Colloid Polym. Sci.* **2018**, *296*, 547–555.
[18] W. Liu, T. Wang, A. G. L. Borthwick, Y. Q. Wang, X. C. Yin, X. Z. Li, J. R. Ni, *Sci. Total Environ.* **2013**, *456*, 171–180.
[19] Q. R. Wang, D. Kim, D. D. Dionysiou, G. A. Sorial, D. Timberlake, *Environ. Pollut.* **2004**, *131*, 323–336.
[20] H. H. Zeng, L. Wang, D. Zhang, P. Yan, J. Nie, V. K. Sharma, C. Y. Wang, *Chem. Eng. J.* **2018**, *358*, 253–263.
[21] D. Zhang, L. Wang, H. H. Zeng, P. Yan, J. Nie, V. K. Sharma, C. Y. Wang, *Chem. Eng. J.* **2019**, *363*, 192–202.
[22] S. Abdulrazak, K. Hussaini, H. M. Sani, *Appl. Water Sci.* **2017**, *7*, 3151–3155.
[23] J. Wang, B. L. Deng, H. Chen, X. R. Wang, J. Z. Zheng, *Environ. Sci. Technol.* **2009**, *43*, 5223–5228.
[24] D. Kweon, J. K. Choi, E. K. Kim, S. T. Lim, *Carbohydr. Polym.* **2001**, *46*, 171–177.
[25] S. Zarei, M. Niad, H. Raanaei, *J. Hazard. Mater.* **2018**, *344*, 258–273.
[26] R. Brion-Roby, J. Gagnon, J. S. Deschênes, B. Chabot, *Pure Appl. Chem.* **2017**, *90*, 63–77.
[27] A. Hanninen, E. Sarlin, I. Lyyra, T. Salpavaara, M. Kellomaki, S. Tuukkanen, *Carbohydr. Polym.* **2018**, *202*, 418–424.

[28] G. Z. Kyzas, D. N. Bikiaris, A. C. Mitropoulos, *Polym. Int.* **2017**, *66*, 1800–1811.
[29] M. Mujtaba, R. E. Morsi, G. Kerch, M. Z. Elsabee, M. Kaya, J. Labidi, K. M. Khawar, *Int. J. Biol. Macromol.* **2019**, *121*, 889–904.
[30] S. Islam, M. A. R. Bhuiyan, M. N. Islam, *J. Polym. Environ.* **2016**, *25*, 854–866.
[31] P. L. Kashyap, X. Xiang, P. Heiden, *Int. J. Biol. Macromol.* **2015**, *77*, 36–51.
[32] A. Soros, J. E. Amburgey, C. E. Stauber, M. D. Sobsey, L. M. Casanova, *J. Water Health* **2019**, *17*, 204–218.
[33] Y. A. Azarova, A. V. Pestov, S. Y. Bratskaya, *Cellulose* **2016**, *23*, 2273–2289.
[34] Y. M. Xu, Y. M. Du, *Int. J. Pharm.* **2003**, *250*, 215–226.
[35] D. G. Trikkaliotis, A. K. Christoforidis, A. C. Mitropoulos, G. Z. Kyzas, *Carbohydr. Polym.* **2020**, *234*, 115890.
[36] Y. K. Zhang, S. S. Chen, X. Z. Feng, J. G. Yu, X. Y. Jiang, *Environ. Sci. Pollut. Res. Int.* **2019**, *26*, 28898–28908.
[37] E. A. M. Azmy, H. E. Hashem, E. A. Mohamed, N. A. Negm, *J. Mol. Liq.* **2019**, *284*, 748–754.
[38] J. D. Chen, Q. W. Liang, S. Ploychompoo, H. J. Luo, *Environ. Sci. Pollut. Res. Int.* **2020**, *27*, 10715–10728.
[39] X. Y. Mao, Y. Y. Duan, C. Y. Wang, *J. Chem. Eng. Data* **2018**, *63*, 4241–4247.
[40] S. Q. Gu, W. Lan, X. Y. Mao, L. P. Yang, C. Y. Wang, *Materials* **2018**, *11*, 514.
[41] K. C. Zhu, Y. Y. Duan, F. Wang, P. Gao, H. Z. Jia, C. Y. Ma, C. Y. Wang, *Chem. Eng. J.* **2016**, *311*, 236–246.
[42] X. Y. Mao, L. Wang, S. Q. Gu, Y. Y. Duan, Y. Q. Zhu, C. Y. Wang, E. Lichtfouse, *Environ. Chem. Lett.* **2018**, *16*, 653–658.
[43] M. Rhazi, J. Desbrières, A. Tolaimate, M. Rinaudo, M. E. Meray, *Eur. Polym. J.* **2002**, *38*, 1523–1530.
[44] D. Zhang, L. Wang, H. H. Zeng, R. Baker, C. Y. Wang, *Environ. Sci. Nano* **2020**, *7*, 793–802.
[45] B. H. Ye, M. L. Tong, X. M. Chen, *Coord. Chem. Rev.* **2005**, *249*, 545–565.
[46] H. Arslanoglu, *Chemosphere* **2018**, *217*, 393–401.
[47] M. S. Islam, S. B. Sharif, J. Lee, U. Habiba, B. C. Ang, A. M. Afifi, *Carbohydr. Polym.* **2016**, *157*, 57–64.
[48] S. X. Duan, X. T. Xu, X. Liu, Y. N. Wang, T. Hayat, A. Alsaedi, Y. D. Meng, J. X. Li, *J. Colloid Interface Sci.* **2018**, *513*, 92–103.
[49] S. Sarode, P. Upadhyay, M. A. Khosa, T. Mak, A. Shakir, S. Song, A. Ullah, *Int. J. Biol. Macromol.* **2018**, *121*, 1086–1100.
[50] D. Xu, W. D. Wu, H. J. Qi, R. X. Yang, W. Q. Deng, *Chemosphere* **2018**, *196*, 174–181.
[51] J. Li, X. D. Li, A. Alsaedi, T. Hayat, C. L. Chen, *J. Colloid Interface Sci.* **2018**, *517*, 61–71.
[52] S. Zarei, M. Niad, H. Raanaei, *J. Hazard. Mater.* **2018**, *344*, 258–273.
[53] H. Asiabi, Y. Yamini, M. Shamsayei, K. Molaei, M. Shamsipur, *J. Hazard. Mater.* **2018**, *357*, 217–225.
[54] I. M. M. Kenawy, M. A. H. Hafez, M. A. Ismail, M. A. Hashem, *Int. J. Biol. Macromol.* **2018**, *107*, 1538–1549.
[55] M. F. Hamza, Y. Z. Wei, A. Benettayeb, X. P. Wang, E. Guibal, *J. Mater. Sci.* **2020**, *55*, 4193–4212.
[56] H. H. Zeng, L. Wang, D. Zhang, F. Wang, V. K. Sharma, C. Y. Wang, *J. Colloid Interface Sci.* **2019**, *554*, 479–487.
[57] M. X. Liu, Y. Zhang, C. C. Wu, S. Xiong, C. R. Zhou, *Int. J. Biol. Macromol.* **2012**, *51*, 566–575.
[58] H. R. Bonne, Y. O. Reyes, M. A. L. Ramalho, *J. Braz. Chem. Soc.* **2007**, *18*, 1388–1396.
[59] B. E. Thacker, D. Xu, R. Lawrence, J. D. Esko, *Matrix Biol.* **2014**, *35*, 60–72.
[60] Y. C. Luo, Q. Wang, *Int. J. Biol. Macromol.* **2014**, *64*, 353–367.
[61] H. E. Knidri, R. Belaabed, A. Addaou, A. Laajeb, A. Lahsini, *Int. J. Biol. Macromol.* **2018**, *120*, 1181–1189.
[62] V. A. Titov, I. M. Lipatova, E. A. Mezina, L. A. Kuz'Micheva, *High Energy Chem.* **2016**, *50*, 411–415.
[63] Z. X. Li, X. Y. Zhou, T. B. Kuang, Z. H. Tian, Q. Liang, *Adv. Mater. Res.* **2014**, *1015*, 393–396.
[64] J. Wang, W. Yao, P. C. Gu, S. J. Yu, X. X. Wang, Y. Du, H. Q. Wang, Z. S. Chen, T. Hayat, X. K. Wang, *Cellulose* **2017**, *24*, 851–861.
[65] R. Brionroby, J. Gagnon, S. Nosrati, J. Deschenes, B. Chabot, *J. Water Proc. Eng.* **2018**, *23*, 13–19.
[66] M. Vakili, M. Rafatullah, B. Salamatinia, A. Z. Abdullah, M. H. Ibrahim, K. B. Tan, Z. Gholami, P. Amouzgar, *Carbohydr. Polym.* **2014**, *113*, 115–130.
[67] J. F. Mendes, R. T. Paschoalin, V. B. Carmona, A. R. S. Neto, A. C. P. Marques, J. M. Marconcini, L. H. C. Mattoso, E. S. Medeiros, J. E. Oliveira, *Carbohydr. Polym.* **2016**, *137*, 452–458.
[68] X. L. Ma, H. Peng, X. Zhang, *Desalin. Water Treat.* **2016**, *57*, 25494–25502.
[69] W. S. W. Ngah, S. Fatinathan, *Colloids Surf. A* **2006**, *277*, 214–222.
[70] S. Lone, D. H. Yoon, H. Lee, I. W. Cheong, *Environ. Sci-Wat. Res.* **2019**, *5*, 83–90.
[71] Z. Fan, B. Y. Yu, Z. R. Yue, T. Wang, W. Xian, Z. B. Liu, C. S. Zhao, *J. Hazard. Mater.* **2007**, *147*, 67–73.
[72] A. Sionkowska, A. P. Anecka, *J. Mol. Liq.* **2013**, *186*, 157–162.
[73] M. M. Beppu, R. S. Vieira, C. G. Aimoli, C. C. Santana, *J. Membr. Sci.* **2007**, *301*, 126–130.
[74] A. A. Naim, A. Umar, M. M. Sanagi, N. Basaruddin, *Carbohydr. Polym.* **2013**, *98*, 1618–1623.
[75] P. Miretzky, A. F. Cirelli, *J. Fluorine Chem.* **2011**, *132*, 231–240.
[76] S. Benamer, M. Mahlous, D. Tahtat, A. Nacerkhodja, M. Arabi, H. Lounici, N. Mameri, *Radiat. Phys. Chem.* **2011**, *80*, 1391–1397.
[77] G. Lofrano, M. Carotenuto, G. Libralato, R. F. Domingos, A. Markus, L. Dini, R. K. Gautam, D. Baldantoni, M. Rossi, S. K. Sharma, *Water Res.* **2016**, *92*, 22–37.
[78] L. Zhang, H. J. Luo, P. P. Liu, W. Fang, J. J. Geng, *Int. J. Biol. Macromol.* **2016**, *87*, 586–596.
[79] D. L. Hall-Edgefield, T. Shi, K. Nguyen, A. Sidorenko, *ACS Appl. Mater. Interfaces* **2014**, *6*, 22026–22033.
[80] X. H. Wang, R. Z. Sun, C. Y. Wang, *Colloids Surf. A* **2014**, *441*, 51–58.

[81] A. P. Mathew, M. P. G. Laborie, K. Oksman, *Biomacromolecules* **2009**, *10*, 1627–1632.
[82] M. Gierszewska, J. Ostrowskaczubenko, *Carbohydr. Polym.* **2016**, *153*, 501–511.
[83] J. Y. Woo, J. H. Oh, S. Jo, C. Han, *ACS Nano* **2019**, *13*, 4522–4529.
[84] M. Gierszewska, J. Ostrowskaczubenko, E. Chrzanowska, *Eur. Polym. J.* **2018**, *101*, 251–290.
[85] L. Y. Chen, P. X. Wu, M. Q. Chen, X. L. Lai, Z. Ahmed, N. W. Zhu, Z. Dang, Y. Z. Bi, T. Y. Liu, *Appl. Clay Sci.* **2018**, *159*, 74–51.
[86] N. F. Elharby, S. M. Ibrahim, N. A. Mohamed, *Water Sci. Technol.* **2017**, *76*, 2719–2732.
[87] P. Yu, H. Q. Wang, R. Y. Bao, Z. Liu, W. Yang, B. H. Xie, M. B. Yang, *ACS Sustainable Chem. Eng.* **2017**, *5*, 1557–1566.
[88] S. Kumari, G. S. Chauhan, *ACS Appl. Mater. Interfaces* **2014**, *6*, 5908–5917.
[89] X. H. Wang, W. Y. Deng, Y. Y. Xie, C. Y. Wang, *Chem. Eng. J.* **2013**, *228*, 232–242.
[90] I. A. Udoetok, R. M. Dimmick, L. D. Wilson, J. V. Headley, *Carbohydr. Polym.* **2016**, *136*, 329–340.
[91] I. A. Udoetok, L. D. Wilson, J. V. Headley, *ACS Appl. Mater. Interfaces* **2016**, *8*, 33197–33209.
[92] L. Mu, S. Yang, B. Hao, P. C. Ma, *Polym. Chem.* **2015**, *6*, 5869–5875.
[93] B. Pan, Y. Wu, J. N. Qin, C. Y. Wang, *Catal. Today* **2019**, *335*, 208–213.
[94] N. Sun, X. Wen, C. J. Yan, *Int. J. Biol. Macromol.* **2018**, *108*, 1199–1206.
[95] A. F. Hassan, R. Hrdina, *Int. J. Biol. Macromol.* **2018**, *109*, 507–516.
[96] K. Kalantari, A. M. Afifi, *Sep. Sci. Technol.* **2018**, *53*, 2527–2535.
[97] L. H. Wang, Y. Y. Qiu, H. J. Lv, Y. Si, L. F. Liu, Q. Zhang, J. P. Cao, J. Y. Yu, X. R. Li, B. Ding, *Adv. Funct. Mater.* **2019**, *29*, 1901407.
[98] B. Y. Li, Y. M. Zhang, D. X. Ma, Z. Shi, S. Q. Ma, *Nat. Commun.* **2014**, *5*, 5537–5545.
[99] H. C. Ge, T. T. Hua, *Carbohydr. Polym.* **2016**, *153*, 246–252.
[100] L. M. Zhou, Z. R. Liu, J. H. Liu, Q. W. Huang, *Desalination.* **2010**, *258*, 41–47.
[101] Z. L. Li, D. Xiao, Y. Y. Ge, S. Koehler, *ACS Appl. Mater. Interfaces* **2015**, *7*, 15000–15009.
[102] M. Monier, *Int. J. Biol. Macromol.* **2012**, *50*, 773–781.
[103] Ö. Acet, T. Baran, D. Erdönmez, N. H. Aksoy, I. Alacabey, A. Mentes, M. Odabasi, *J. Chromatogr. A.* **2018**, *1550*, 21–27.
[104] G. S. Shaw, K. Uvanesh, S. N. Gautham, V. Singh, K. Pramanik, I. Banerjee, N. Kumar, K. Pal, *Des. Monomers. Polym.* **2015**, *18*, 434–450
[105] T. Phothitontimongkol, N. Siebers, N. Sukpirom, F. Unob, *Appl. Surf. Sci.* **2009**, *43*, 343–349.
[106] A. J. Tchinda, E. Ngameni, I. Kenfack, A. Walcarius, *Chem. Mater.* **2009**, *21*, 4111–4121.
[107] L. Tran, P. X. Wu, Y. J. Zhu, S. Liu, N. W. Zhu, *Appl. Surf. Sci.* **2015**, *356*, 91–101.
[108] W. Wang, Y. L. Zhao, H. Y. Bai, T. T. Zhang, V. Ibarra-Galvan, S. X. Song, *Carbohydr. Polym.* **2018**, *198*, 518–528.
[109] Y. L. Ma, L. Lv, Y. R. Guo, Y. J. Fu, Q. Shao, T. T. Wu, S. J. Guo, K. Sun, X. K. Guo, E. K. Wujcik, Z. H. Guo, *Polymer* **2017**, *128*, 12–23.
[110] Y. Y. Wang, X. H. Wang, Y. M. Ding, Z. L. Zhou, H. Chen, S. S. Zhou, *Powder Technol.* **2018**, *325*, 597–605.
[111] Ł. Klapiszewski, K. Siwinskastefanska, D. Kolodynska, *Chem. Eng. J.* **2017**, *314*, 169–181.
[112] Y. Q. Jin, C. M. Zeng, Q. F. Lv, Y. Yu, *Int. J. Biol. Macromol.* **2018**, *123*, 50–58.
[113] L. Qin, Y. Y. Ge, B. W. Deng, Z. L. Li, *J. Taiwan Inst. Chem. E.* **2016**, *71*, 84–90.
[114] S. Deng, G. S. Zhang, S. Liang, P. Wang, *ACS Sustainable Chem. Eng.* **2017**, *5*, 6054–6063.
[115] L. J. Ma, Q. Wang, S. M. Islam, Y. C. Liu, S. Ma, M. G. Kanatzidis, J. Am, *Chem. Soc. Rev.* **2016**, *138*, 2858–2866.
[116] X. H. Wang, W. Deng, Y. Y. Xie, C. Y. Wang, *Chem. Eng. J.* **2013**, *228*, 232–242.
[117] S. Ahmed, J. Brockgreitens, K. Xu, A. Abbas, *Adv. Funct. Mater.* **2017**, *27*, 1606572.
[118] M. Monier, *Int. J. Biol. Macromol.* **2012**, *50*, 773–781.
[119] G. Kyzas, E. Deliyanni, *Molecules* **2013**, *18*, 6193–6214.
[120] X. H. Wang, W. Y. Deng, Y. Y. Xie, C. Y. Wang, *Chem. Eng. J.* **2013**, *228*, 232–242.
[121] H. C. Ge, T. T. Hua, *Carbohydr. Polym.* **2016**, 246–252.
[122] O. A. Oyetade, A. A. Skelton, V. O. Nyamori, S. B. Jonnalagadda, B. S. Martincigh, *Sep. Purif. Technol.* **2017**, *188*, 174–187.
[123] A. Mielcarek, A. Dołęga, *J. Mol. Struct.* **2016**, *1103*, 217–223.
[124] Y. Z. Niu, J. Y. Yang, R. J. Qu, Y. H. Gao, N. Du, H. Chen, C. M. Sun, W. X. Wang, *Ind. Eng. Chem. Res.* **2016**, *55*, 3679–3688.
[125] S. Chandrasekar, V. Balachandran, H. S. Evans, A. Latha, *Spectrochim. Acta Part A* **2015**, *143*, 136–146.

RECORD REVIEW

Chitosan is an excellent bio-adsorbent for metal ions removal because of the large number of $-NH_2$ groups. A series of chitosan derivatives have been obtained by crosslinking with glutaraldehyde among others or by grafting new functional groups on the chitosan backbone with the aim of adsorbing Hg (II) ions. The new functional groups allow to change the pH range for Hg(II) ions adsorption, to change the adsorption sites in order to increase adsorption capacity and efficiency, and to enhance sorption selectivity.

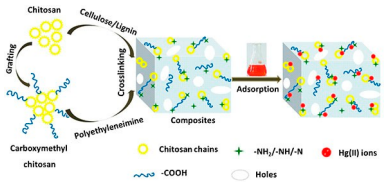

*D. Zhang, G. Crini, E. Lichtfouse, B. Rhimi, C. Wang**

1 – 16

Removal of Mercury Ions from Aqueous Solutions by Crosslinked Chitosan-based Adsorbents: A Mini Review